Journal of Materials Science: Materials in Medicine (2018) 29:137
https://doi.org/10.1007/s10856-018-6146-1

ENGINEERING AND NANO-ENGINEERING APPROACHES FOR MEDICAL DEVICES

Original Research

# Electrospun polylactic acid-chitosan composite: a bio-based alternative for inorganic composites for advanced application

Merin Sara Thomas[1,2,3] · Prasanth K. S. Pillai[4] · Marisa Faria[5,6] · Nereida Cordeiro[5,6] · Hernane Barud[7] · Sabu Thomas[1] · Laly A. Pothen[1,3]

Received: 14 February 2018 / Accepted: 1 August 2018 / Published online: 17 August 2018


## Abstract

Fabricating novel materials for biomedical applications mostly require the use of biodegradable materials. In this work biodegradable materials like polylactic acid (PLA) and chitosan (CHS) were used for designing electrospun mats. This work reports the physical and chemical characterization of the PLA–CHS composite, prepared by the electrospinning technique using a mixed solvent system. The addition of chitosan into PLA, offered decrease in fiber diameter in the composites with uniformity in the distribution of fibers with an optimum at 0.4wt% CHS. The fiber formation and the reduction in fiber diameter were confirmed by the SEM micrograph. The inverse gas chromatography and contact angle measurements supported the increase of hydrophobicity of the composite membrane with increase of filler concentration. The weak interaction between PLA and chitosan was confirmed by Fourier transform infrared spectroscopy and thermal analysis. The stability of the composite was established by zeta potential measurements. Cytotoxicity studies of the membranes were also carried out and found that up to 0.6% CHS the composite material was noncytotoxic. The current findings are very important for the design and development of new materials based on polylactic acid-chitosan composites for environmental and biomedical applications.

## Graphical Abstract

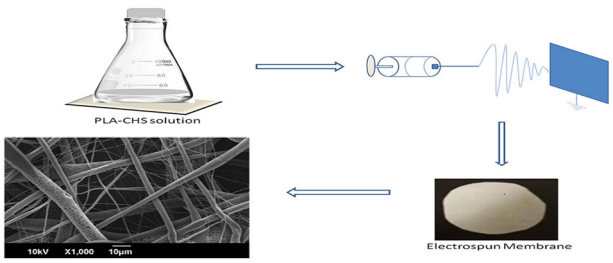


✉ Laly A. Pothen
lapothan@gmail.com

[1] International and Interuniversity Centre for Nanoscience and Nanotechnology, Mahatma Gandhi University, Priyadarsini Hills P.O., Kottayam, Kerala 686 560, India

[2] Department of Chemistry, Mar Thoma College, Kuttapuzha P.O., Tiruvalla, Kerala 689103, India

[3] Department of Chemistry, C.M.S. College, Kottayam, Kerala 686001, India

[4] Food and Bioproduct Sciences, University of Saskatchewan, Saskatoon, SK S7N0W4, Canada

[5] Faculty of Exact Science and Engineering, University of Madeira, 9000-390 Funchal, Portugal

[6] CIIMAR, University of Porto, 4450-208 Matosinhos, Portugal

[7] Institute of Chemistry-UNESP, CP 355, Zip 14801-970, Araraquara, SP 14801-970, Brazil

## 1 Introduction

Natural polymers, particularly cellulose, chitin, starch etc., are environmental friendly, biodegradable and sustainable and can be disposed of or composted easily without harming the environment [1, 2]. Due to these attractive properties, these natural polymers are driving modern industrial economies and have been widely used in pharmaceuticals, construction, adhesives, food, food packaging, beverage industries, cosmetics, toiletries, paint and ink industries [3–9]. Every year about $17 \times 10^{10}$ metric tonnes of biomass are produced by nature, of which only 3.5% are exploited by mankind [10]. Although the consumption of natural polymers is about 2% of the 300 million tons of plastics produced per year, their production is steadily rising. The production of bio based polymers in the commercial sector is escalating and it is going to reach 17 million tons in 2020 [11].

Polylactic acid (PLA) and chitosan are two polymers that are biodegradable and possess excellent biocompatibility and biodegradability [12]. PLA is a linear aliphatic thermoplastic polyester, derived from renewable resources such as beet, corn and sugar [13]. Nowadays PLA-based biocomposites can compete with the petroleum-based plastics that are available in the market because of the increased availability of PLA and growing petroleum costs [14]. Excellent mechanical properties, transparency, biodegradability, resistance to fats and oil and the wide availability have made PLA as an excellent candidate for a variety of applications. Hydrophobic PLA composites are widely used for food packaging [15] as well as for the cardiovascular implants [16] due to their recyclability and biodegradability. A series of devices were prepared from different PLA types, including degradable sutures, drug releasing micro-particles, nano-particles, and porous scaffolds for cellular applications [17]. Sakai et al. [18] fabricated polylactide-based biodegradable thermoset scaffolds for tissue engineering applications. Li et al. [19] found that the scaffolds were porous with good interconnectivity and thermal stability, and evaluated the efficacy and feasibility of PLA ureteral stents for the treatment of ureteral war injuries. The stents made of PLA were reliable in the treatment of ureteral war injuries where PLA stents were degraded so that they were removed from the body. Therefore, PLA stents represented a promising future for the treatment of ureteral war injuries.

Chitosan (CHS) is the deacetylated derivative of chitin which is abundantly available in the exoskeletal waste of crustaceans. The biodegradability, biocompatibility and nontoxic nature of chitosan make it a safer material for a wide range of environmental and biomedical applications [20, 21]. Chitin and chitosan exist in various applied forms like hydrogels, membranes, nanofibers, beads, micro/nanoparticles, scaffolds, and sponges. Biodegradability; predictable degradation rate; structural integrity; non-toxicity to cells; and biocompatibility made chitin to be good wound healing, tissue engineering, and in lenses fabrication for ophthalmology [21–23]. Due to the poly cationic nature of the chitosan it can interact with the surface of cell membrane and can be used as a bone tissue regeneration material [24], an analgesic [25], bone regeneration [26] etc.

Electrospinning is a simple, versatile technique used for the production of polymeric fibres having micro to nano dimensions. This process is remarkably efficient, rapid, and inexpensive and produces fibres with high surface area to volume ratio, high porosity and small pore size [27]. Also, the polymeric materials that are fabricated by electrospinning method allow different fiber morphologies, such as round, flat, smooth and beaded etc. The influence of molecular weight and viscosity of spinning solutions on the fiber thickness was demonstrated by Tomaszewski et al [28]. In recent years the study of electrospun chitosan nanofibers has received great attention because of its inherent antibacterial activity. Pure chitosan fibers can be prepared using trifluoroacetic acid (TFA) [29] as a solvent and a bicomponent blend of chitosan with PEO [30], PLA [31], PCL [32], and PVA [33]. Sonseca et al. [34] prepared biodegradable polylactide/hydroxyapatite nanofibers via electrospinning. In a study by Xu et al. [35], human vascular endothelial cells cultured on smooth solvent-cast PLA surface were shown to be more than on the rough electrospun surface.

In our present work, we prepared PLA–CHS composites by means of electrospinning method to produce biocomposite fibers. The main aim of this work was to prepare environmental friendly composites using a mixed solvent system of chloroform and acetic acid, which yields a smooth and hydrophobic structure with noncytotoxicity. The current synthetic strategy can produce composites that are extremely useful for biomedical applications. Also, the study extends its objective to check the suitability of these composites for environmental and packaging applications. The fibre formation was confirmed by the SEM analysis. The Inverse Gas Chromatography (IGC) and contact angle measurements were used to analyse the hydrophobicity of the membranes and Zeta potential for stability of the membranes. The interaction between PLA and chitosan was confirmed by Fourier transform infrared spectroscopy analysis and the thermal studies of the composites were done by thermal gravimetric analysis (TGA) and differential scanning calorimetry (DSC). Cell Viability studies of these composites were also done.

## 2 Materials and methods

### 2.1 Materials

Polylactic acid (PLA) was supplied by Shenzen Bright China Industrial Co. Ltd, China and has a density of 1.24 g/cm$^3$ and the melt flow index (MFI) of 20 g/10 min at 190 °C/2.16 kg, reported by the supplier and the chitosan (medium molecular weight) supplied by Marine chemicals, Cochin, Kerala, India. Chloroform (99% purity) and glacial acetic acid (>99% putity) were purchased from Merck chemicals, India and are of commercial grade. Methane had the high purity (>99.99%) and were supplied by Air Liquide Company, France. Acetonitrile (ACN), ethyl acetate (EtOAc), ethanol (EtOH), acetone (AC) and tetrahydrofuran (THF) all GC grade (>99% purity) were purchased from Sigma- Aldrich. 10% fetal bovine serum, tetrazolium 3-(4,5-dimethylthiazol-2-yl)-2,5-diphenyl tetrazolium bromide, dimethyl sulfoxide, isopropyl alcohol, phosphate buffered saline (1× PBS), Double distilled water were also used. All the chemicals purchased are used without further treatment.

### 2.2 Analytical methods

#### 2.2.1 Electrospinning

Electrospinning method (Holmarc, HO-NFES-040D) was adapted to prepare PLA–CHS fibers from PLA in chloroform and chitosan in acetic acid. The two solutions were mixed well using a magnetic stirrer (600 rpm) for 24 h and then ultrasonicated (MSW-269) for 20 min just before electrospinning. The distance between the needle tip and metallic collector was adjusted to 15 cm, and the applied voltage over the gap was kept 15 kV. The PLA–CHS solution was fed by a syringe pump with a flow rate of 1 mL/h.

#### 2.2.2 Scanning electron microscopy (SEM)

The surface morphology of the samples was analyzed by SEM imaging. The micrographs of the spun fibres were taken in JEOL, Model JSM 6390 (Japan) electron microscope with an accelerating voltage of 10 kV. The samples were coated with platinum to avoid the electrostatic charge dissipation. ImageJ (version 1.44) software was used for the characterization of the SEM micrographs.

#### 2.2.3 Fourier transform infrared spectroscopy (FTIR)

FTIR spectra of the membranes were obtained using a recorded using SPECTRUM 400 FT-IR spectrometer equipped with attenuated total reflectance (ATR) system. The samples were loaded onto the ATR crystal area and held in place by a pressure arm. The spectra were acquired over a scanning range of 4000–500 cm$^{-1}$ for 15 repeated scans at a spectral resolution of 4 cm$^{-1.}$

#### 2.2.4 Thermogravimetric analysis (TGA)

The TGA measurements were carried out on a Q500 model (TA Instruments, DE, USA) under dry nitrogen of 40 mL/min for balance purge flow and 60 mL/min for sample purge flow. Approximately 8.0–15.0 mg of sample was loaded into the open TGA platinum pan then heated from 25 °C to 600 °C at a constant rate of 10 °C/min.

#### 2.2.5 Differential scanning calorimetry (DSC)

The thermal transition behavior of the samples was investigated using a Q200 model (TA Instruments, New Castle, DE) by modulated DSC following ASTM E1356-03 standard. The sample (3.0–6.0 mg) in hermetically sealed aluminum DSC pan was first equilibrated at 25 °C and heated to 150 °C at 10 °C/min (first heating cycle). The sample was held at that temperature for 10 min and then cooled down to 0 °C at 10 °C/min, and subsequently reheated to 150 °C at the same rate (second heating cycle). Modulation amplitude and period were ± 1 °C and 60 s, respectively. The "TA Universal Analysis" software version 5.4 was used to analyze the TGA and DSC thermograms. The characteristics of non-resolved peaks were obtained using the first and second derivatives of the differential thermogravimetry (DTG) and differential heat flow.

#### 2.2.6 Inverse gas chromatography (IGC)

IGC measurements were carried out on a commercial inverse gas chromatography that is equipped with flame ionization (FID) and thermal conductivity (TCD) detectors. The IGC system was fully automatic with SMS IGC Controller V 1.8 Control Software. Data analysis was done using IGC Standard Analysis Suite V 1.3 and IGC Standard Analysis Suite V 1.21. The columns used were standard glass silanized (dimethyldichlorosilane; Repelcote BDH, UK) with 300 mm length and an internal diameter of 3 mm. The samples were packed in the columns by vertical tapping for 2 h using the SMS sample packing device and conditioned over-night at 313 K followed by 2 h at temperature analysis. The dispersive component of the surface free energy were determined by applying four *n*-alkanes: heptane, octane, nonane and decane at four temperatures: 293, 298, 303 and 308 K. ACN, EtOAc, EtOH, AC and THF were the polar molecules used for the determination of the specific free energy and acid-base surface character. The *n*-octane was used as the probe molecule to determine the

parameters of isotherm, permeability and diffusion experiments. All the measurements were carried out at 0% relative humidity, a helium flow rate of 10 mL/min, and in duplicate, producing an experimental error below 2%. Methane was used as reference molecule for calculation of dead time and helium was used as carrier gas with a flow rate of 10 mL/min.

#### 2.2.7 Zeta potential measurements

Zeta potential analysis was done using Zeta potential Analyzer (Zetasizer 300 HAS, Malvern Instruments, Worcestershire, UK). All measurements in this study were taken at a temperature of 25 °C. At least three replicate analysis on each sample were done to check the reproducibility of the result. PLA, CHS and Composites were dispersed in suitable solvent and the zeta potential measurement was taken using Zetasizer.

#### 2.2.8 Contact angle measurement

The surface contact angles were measured by SEO Phoenix 300 using software-8. A computer controlled automatic micro syringe system was used to dispense a 6–7 µL droplet of deionized water over the surface of the film. A picture of the drop was captured after the drop was set onto the sample. The contact angle is measured as the tangent angle formed between a liquid drop and its supporting surface. The contact angles could be calculated by the software through analyzing the shape of the drop. The contact angle θ was an average of 50 measurements. Contact angle measurements of nanocomposites of PLA with chitosan were done at room temperature with distilled water. Total surface free energy from these measurements were calculated. At first, the contact angles were measured for each sample for at least six to ten times. The average is taken as the contact angle for the particular sample.

#### 2.2.9 Cytotoxicity studies

PLA and PLA/CHS membranes (concentrations of 0.2, 0.4%, 0.6 and 0.8% w/w) were weighed, minced, sterilized in UV radiation, immersed in cell culture Dulbeccos Modified Eagle's Medium (DMEM-Vitrocell) supplemented with 10% fetal bovine serum (FBS-Vitrocell) and antibiotics (Penicillin and Streptomycin - Vitrocell), subjected to intense mechanical agitation and stored at 37 °C for 24 h. After these steps, the resultant medium were removed and replaced in cell culture plate wells (96 wells) containing human fibroblast cell lineage (GM07492) at density $15 \times 10^3$ cells/well. The plates were kept in cell culture incubator (Panasonic-$CO^2$ incubator MOC-19 AIC-UV) at 37 °C, humidified atmosphere containing 5% $CO_2$ and 95% air atmosphere for 24 h. Cell viability was determined by the MTT-formazan (tetrazolium 3-(4,5-dimethylthiazol-2-yl)-2,5-diphenyl tetrazolium bromide) colorimetric method. The culture medium was removed from the wells and they were washed with phosphate buffered saline (1× PBS). Aliquots of 50 µL of MTT (SIGMA 2128) was added to each well and the cells were kept in ideal culture conditions for 4 h. After this period, 100 uL of isopropyl alcohol were added in each well and the content mechanically homogenized until complete solubilization of the formazan crystals. The optical density values (OD) were obtained using a spectrophotometer (Polaris-CELER) at 570 nm. The value measured in experimental groups (PLA and PLA/CHS membranes) were converted into percentages of cell viability relative to a control group (−Control) and subjected to statistical variance analysis (ANOVA-ONE WAY), with 5% level of significance ($P \leq$ (Pnif. Cytotoxic activity was considered in values of cell viability percentage ≤70%. A cytotoxic control group (+Control) was included using standard culture medium with 30% (v/v) of Dimethyl Sulfoxide (DMSO-SIGMA 276855).

## 3 Results

### 3.1 SEM characterization

Electrospinning of 12.5 wt% PLA give rise to bead free fibres with porous structure (Fig. 1). The SEM micrographs and the fiber distribution curve of PLA fibrous mat with different wt% of CHS loading is given in Figs. 2 and 3. After filler loading the diameter of the fibres become decreased.

### 3.2 FTIR characterization

PLA fiber mat, CHS and PLA –CHS composite were analyzed using FTIR spectroscopy to observe the changes in chemical composition of fibers before and after the introduction of CHS (Fig. 4) and observed that the chemical composition of neat fibers was not significantly affected by CHS due to the very low concentration of CHS.

### 3.3 Thermal properties of PLA and PLA–CHS composites

DSC and TGA tests were conducted to gain thermal properties of PLA and PLA–CHS fiber mats (Figs. 5 and 6) and found that the thermal transitions are not very much affected by CHS because of the minimal interaction between the filler and PLA.

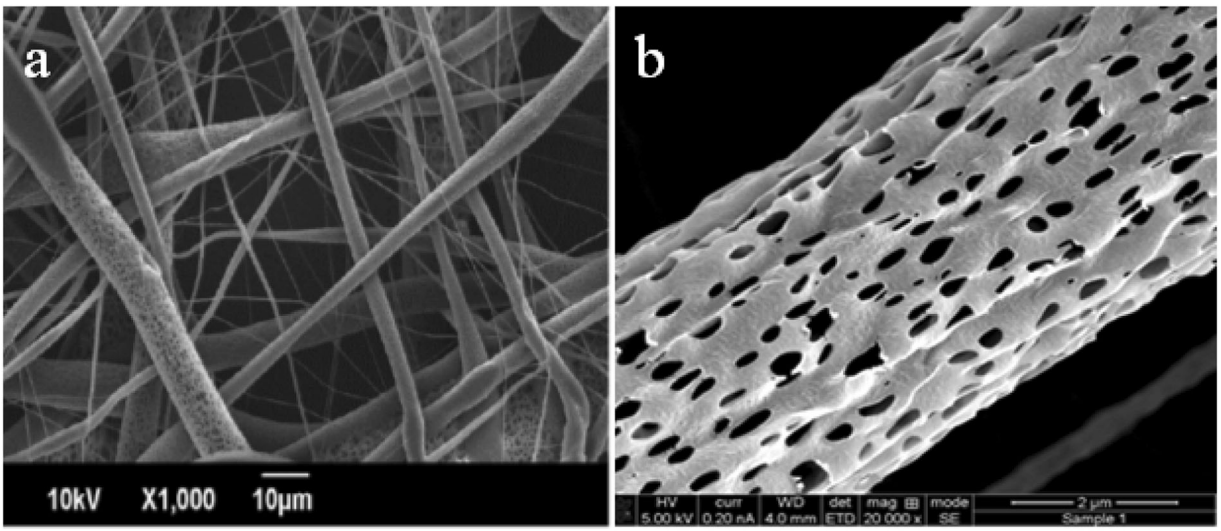


**Fig. 1** **a** SEM picture of neat PLA, **b** high resolution SEM image of neat PLA

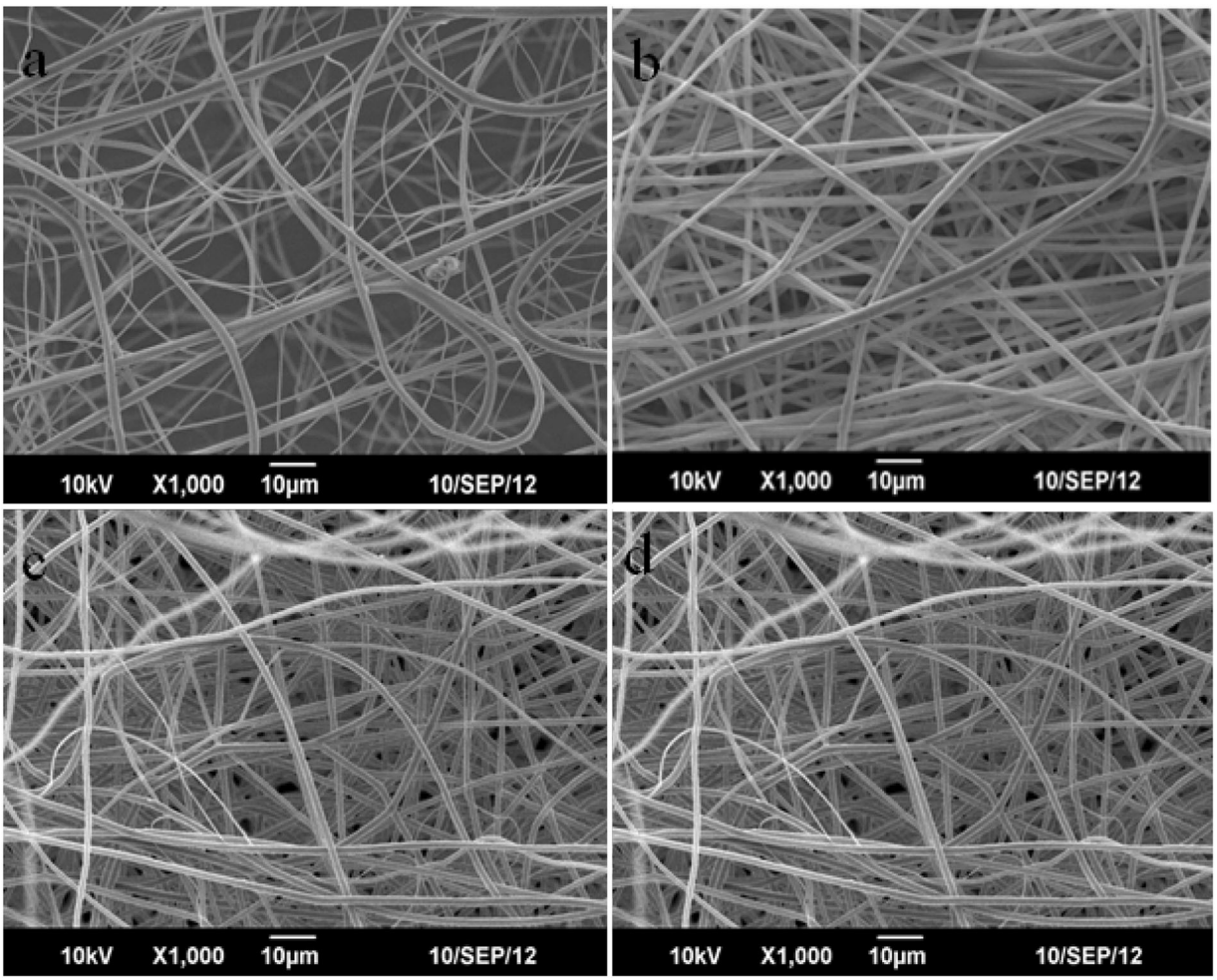


**Fig. 2** SEM images of **a** PLA+0.2 wt% CHS, **b** PLA+0.4 wt% CHS, **c** PLA+0.6 wt% and **d** PLA+0.8 wt% CHS

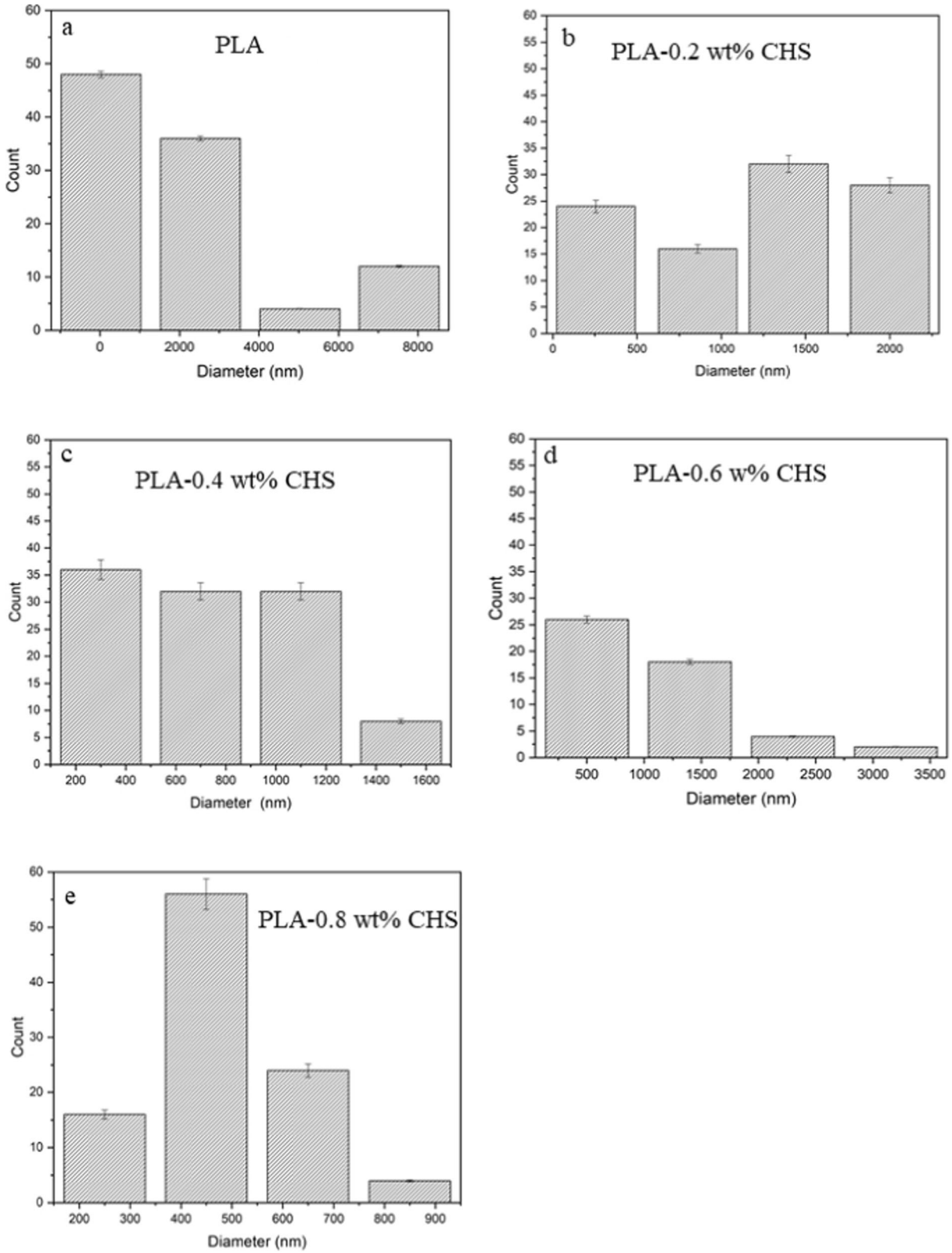


**Fig. 3** Fibre distribution curves of **a** PLA, **b** PLA+0.2 wt% CHS, **c** PLA+0.4 wt% CHS, **d** PLA+0.6 wt% and **e** PLA+0.8 wt% CHS

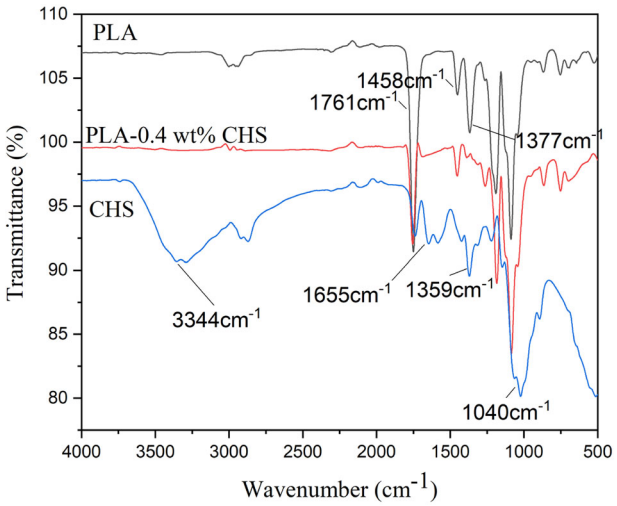


**Fig. 4** FTIR spectra of PLA, chitosan and PLA–chitosan composites

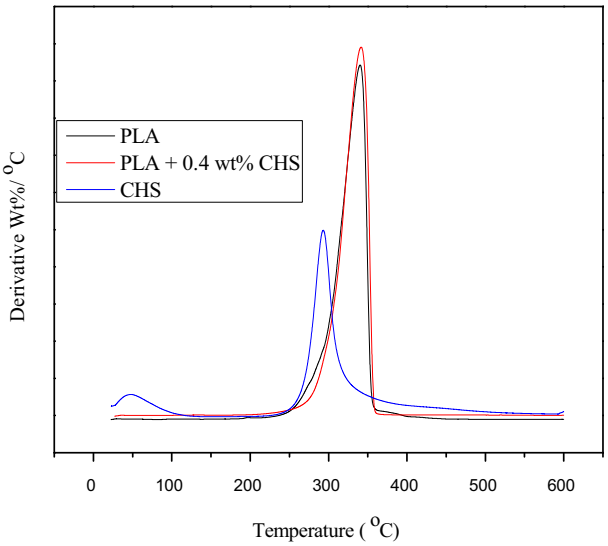


**Fig. 5** TGA curve of PLA, chitosan and PLA–chitosan composites

### 3.4 Inverse gas chromatography experiments

In order to understand the nature of PLA–CHS interactions and their effect on surface properties, the fiber mats were analyzed by IGC. Through non-polar and polar probe molecules, the dispersive component of surface energy ($\gamma^{D}_{S}$) (Table 1); specific surface area ($S_{BET}$), monolayer capacity ($n_m$), diffusion coefficient ($D_p$), and maximum of adsorption potential distribution (Amax) (Table 2) and acid base constants for the fiber mats ($K_A$ and $K_B$) (Table 3) were determined.

### 3.5 Zeta potential measurements

Results of zeta potential for measuring the surface charge of PLA and PLA–CHS composite fibers were recorded in Table 4. The results showed that the composites are more stabilized than PLA up to 0.4 wt%.

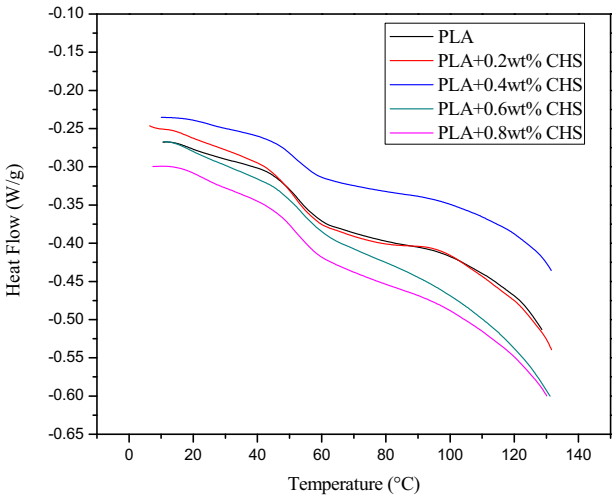


**Fig. 6** DSC curve for PLA and PLA–CHS composites

### 3.6 Contact angle measurements

The water contact angle measurement was performed to evaluate the surface wettability of the fiber mats Fig. 7 and found that addition of CHS decreased the hydrophilicity of the web. The surface energy of the system also obtained from the contact angle measurements Fig. 8. It gives the energy associated with the interface between two phases.

### 3.7 Cytotoxicity assay

To study the cytotoxicity of the prepared fibre mats, MTT-formazan viability/cytotoxicity in vitro assay carried out according to the method described. Figure 9 represents the results of this assay and according to this figure, upto 0.6wt % of chitosan loading the composite webs are non-cytotoxic.

## 4 Discussions

### 4.1 SEM characterization

Figure 1a represents the SEM micrograph of electrospun PLA mat and Fig. 1b shows the high-resolution SEM micrograph of the same. It was observed that there were pores in the PLA fibers (see Fig. 1b), which is due to the condensation of water droplets on the surface of a polymer solution [35]. The breath figures indicates the evaporative cooling of solvent on the surface of the spun fibers (see Fig. 1b), which might happened during the path of the polymer jet from needle tip to collector, where the water vapour

**Table 1** Dispersive surface energy ($\gamma^{D}_{S}$) and its variations with temperature of chitosan and PLA films

| Samples | $\gamma_S^D$ (mJ/m$^2$) | | | | $\left(-\frac{\Delta\gamma_S^D}{\Delta T}\right)$(mJ m$^{-2}$/K) |
|---|---|---|---|---|---|
| | 293 K | 298 K | 303 K | 308 K | |
| CHS | 42.71 ± 1.28 | 41.02 ± 1.23 | 39.63 ± 1.32 | 39.39 ± 1.11 | 0.22 ± 0.007 |
| PLA | 38.30 ± 1.24 | 37.62 ± 1.41 | 37.13 ± 1.11 | 36.80 ± 1.48 | 0.10 ± 1.48 |
| PLA+0.4CHS | 37.02 ± 0.90 | 35.70 ± 1.00 | 34.59 ± 0.87 | 33.63 ± 1.01 | 0.23 ± 0.009 |
| PLA+0.8CHS | 37.27 ± 1.01 | 36.59 ± 1.21 | 36.26 ± 1.42 | 35.60 ± 1.68 | 0.11 ± 0.003 |

**Table 2** Specific surface area ($S_{BET}$; m$^2$/g), monolayer capacity ($n_m$; µMol/g), diffusion coefficient ($D_p$; µcm$^2$/s), and maximum of adsorption potential distribution (Amax; KJ/Mol) of CHS and PLA films, at 298 K

| Samples | $S_{BET}$ | $n_m$ | $A_{max}$ | R | $D_p$ | R |
|---|---|---|---|---|---|---|
| CHS | 0.83 ± 0.03 | 2.18 ± 0.11 | 10.4 ± 0.63 | 0.9984 | 9.023 ± 0.379 | 0.9803 |
| PLA | 3.07 ± 0.18 | 8.08 ± 0.72 | 13.9 ± 0.44 | 0.9994 | 8.586 ± 0.318 | 0.9938 |
| PLA+0.4CHS | 2.10 ± 0.09 | 5.53 ± 0.11 | 16.9 ± 0.67 | 0.9940 | 3.698 ± 0.199 | 0.9483 |
| PLA+0.8CHS | 2.25 ± 0.06 | 5.93 ± 0.26 | 14.3 ± 0.72 | 0.95037 | 1.091 ± 0.041 | 0.9853 |

**Table 3** Acid base constant ($K_A$ and $K_B$) obtained for fibers PLA, chitosan and modified fibers at 298 K

| Samples | $K_A$ | $K_B$ | $K_B/K_A$ | Correlation coefficient |
|---|---|---|---|---|
| CHS | 0.07 | 0.07 | 1.0 | 0.9956 |
| PLA | 0.10 | 0.13 | 1.3 | 0.9852 |
| PLA+ 0.4CHS | 0.12 | 0.21 | 1.8 | 0.9680 |
| PLA+ 0.8CHS | 0.11 | 0.15 | 1.4 | 0.9869 |

**Table 4** Zeta potential values of PLA, chitosan and composites

| Materials | Zeta potential (mV) |
|---|---|
| PLA | 3.36 ± 0.64 |
| CHS | 60.2 ± 0.5 |
| PLA-0.2CHS | 5.98 ± 0.18 |
| PLA-0.4CHS | 9.87 ± 0.42 |
| PLA-0.6 CHS | 1.51 ± 0.58 |
| PLA-0.8CHS | 1.13 ± 0.12 |

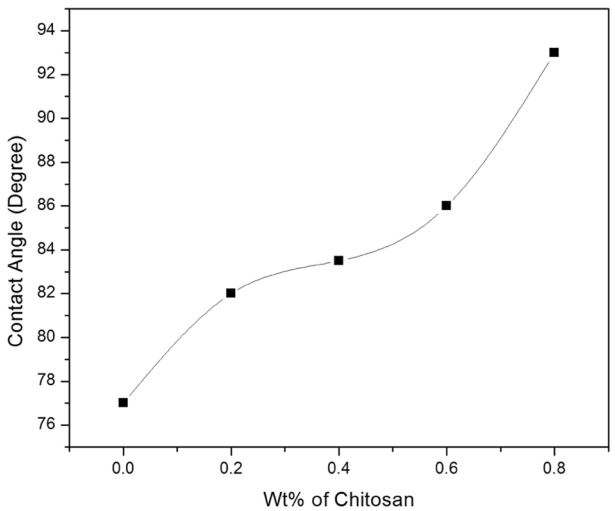


**Fig. 7** The variation of contact angle of water with respect to filler loading

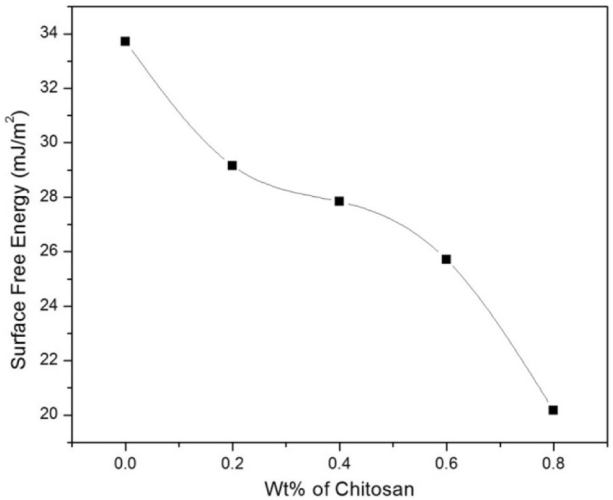


**Fig. 8** The variation of surface free energy with respect to filler loading

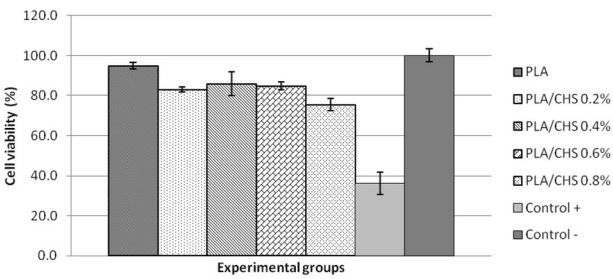


**Fig. 9** MTT-formazan viability/cytotoxicity in vitro assay of PLA and PLA/CHS membranes (concentrations of 0.2%, 0.4%, 0.6% and 0.8% w/w) performed with human fibroblast lineage (GM07492). −Control: cells cultured in standard medium (DMEM supplemented with FBS–10% v/v). +Control: cells cultured in DMSO and standard medium (30% v/v). Results are expressed as percentage of cell viability relative to −Control group

present in the atmosphere condenses on the surface of the fibres creating an imprint on the surface. The porous structure can also be explained in terms of phase separation behaviour via spinodal decomposition. During electrospinning process there generate polymer- rich and solvent- rich regions due to the thermodynamic instability of the spinneret. The polymer rich region solidifies more quickly than the solvent rich region and hence pores were formed [36]. Both these two effects contribute to the porosity of the individual fibres.

The electrostatic attraction between the biopolymers and the conductivity of the solvent systems are the two factors that drives the electrospinning process, and any factor that enhances the charge density will result in the formation of fibres having narrow diameter [37]. Thus, with increased addition of CHS (see Figs. 2 and 3), we obtained uniform fibers with decreased diameter. This is due to the increase in charge density of polymer solutions with increased filler concentration [38] or by the use mixed solvent system that possess higher conductivity than individual chloroform and acetic acid [39]. It was observed that 0.4 wt% CHS loading was the optimum amount, and further loadings has caused decrease in the uniformity of the fiber dimension (there is reduction in diameter size). Figure 3 corresponds to the fibre diameter distribution graphs based on SEM images. From the fibre distribution graph, it was obvious that PLA with 0.4 wt% of chitosan have uniform diameter distribution.

As we can see in Fig. 2, some dumbbell shaped deformations on the fibre surface of the composites, which was occurred due to the large difference in the boiling point (b.p of chloroform: ~61 °C ; b.p of acetic acid: ~118 °C) of the system by the application of mixed solvent system [23]. During the process of fibre formation, chloroform (boiling point ~61 °C) evaporates rapidly resulting in the formation of a "rigid" coating on the fibre surface, while acetic acid (boiling point ~118 °C) evaporates slowly and is entrapped inside the fiber. With further evaporation of the mixed solvents, the tubular fiber structure begins to collapse, and the resulting uneven surface (or interface) produces tangential stress due to the Marangoni effect (the mass transfer along an interface between two fluids due to surface tension gradient) [39]. This causes the deformation of the fibers and results such type dumbbell-like region on fiber surface. Therefore, the formation of such flat PLA fibers with dumb bell surface structure made the fibre surfaces rough and the reason for hydrophobicity of the material.

### 4.2 FTIR characterization

Figure 4, represents the FTIR spectra of CHS, PLA, PLA–CHS composites. The characteristic broad band around 3500–3100 $cm^{-1}$ was the stretching vibrations -OH and –NH of chitosan. The –NH bend vibrations in primary amines was confirmed by the peaks at 1655 $cm^{-1}$ (CO–NHR) and 1574 $cm^{-1}$ ($NH_2$), while, the amide (C–N) band appears around 1359 $cm^{-1}$ [40]. The ester linkage in PLA was confirmed by the characteristic band at 1761 $cm^{-1}$. As seen in Fig. 4, it was noted that all the peak positions are same for both PLA and PLA–CHS composites but the intensity of ester linkage (1761 $cm^{-1}$) of PLA decreased in the case of composites. This indicates the presence of CHS in PLA and the molecular interaction between chitosan and PLA was weak because PLA does not have enough −OH groups to form hydrogen bonds with –OH groups and $-NH_2$ groups in chitosan [41]. Peaks around 1040 $cm^{-1}$ attribute to the stretching of C–$CH_3$ in PLA [42]. The region between 1500 and 1452.3 $cm^{-1}$ significant for $CH_3$ group [43]. There is a development of a small peak just below the carbonyl peak at 1650 $cm^{-1}$. This is an O–H peak that originated from bending of the unresolved hydroxyl group of the absorbed water usually carried by the filler [44, 45]. The composite do not show any characteristic peak corresponding to the –NH or –OH stretching (3500–3100 $cm^{-1)}$ in chitosan. This is because of the very low concentration of chitosan in composites [45].

### 4.3 Thermal properties of PLA and PLA–CHS composites

Figure 5 shows the DTG profiles of the neat PLA and PLA–CHS composites. The DTG curves of the composites showed one prominent decomposition pattern (indicated by their peak temperatures in Fig. 5) indicating a single stage decomposition process. The temperature of degradation of PLA determined at 5 and 10% weight loss ($T_{5\%}$ and $T_{10\%}$, respectively) were ~275 °C, 290 °C, respectively. The addition of fillers enhanced the thermal stability in the composites approximately by 10 °C. This means that incorporation of the CHS induced the thermal stability of pure PLA. Similar results was also reported by Haafiz et al. [46] when they studied PLA composites reinforced with oil palm biomass microcrystalline cellulose. The improved of thermal stability was maximum for 0.6% addition of CHS instead of PLA with 0.4wt% CHS having uniform fiber distribution due to this increased amount of chitosan content. Unlike the onset decomposition temperatures, the main decomposition step in composites and PLA were occurred at almost similar temperature (340 ± 2 °C).

Figure 6 shows the DSC profiles obtained during the second heating cycle of PLA and PLA–CHS composites. Glass transition temperature ($T_g$) is commonly identified as a complex phenomenon that relies on several factors such as intermolecular interaction, chain flexibility and molecular weight of the material itself. The DSC thermogram of neat PLA and the composites displayed one inflection point

indicating a glass transition at ~50 ± 2 °C. Since there is no significant change observed in the glass transitions between neat PLA and the corresponding composites, the observed glass transition might be due to the molecular motion of the soft segments in PLA. The addition of fillers has minimal interactions with PLA matrix and hence didn't affect the thermal transition of the corresponding composites. The minimal interaction between PLA and CHS may be due to insufficient hydroxyl groups in PLA to form hydrogen bonds with −OH groups and $-NH_2$ groups in chitosan [47].

### 4.4 Inverse gas chromatography experiments

The IGC analysis of PLA, CHS and PLA–CHS composites were executed for explaining the surface energy of the system. The dispersive surface energy ($\gamma^D_S$) is directly proportional to hydrophilicity and is inversely proportional to the temperature hence is important to predict the hydrophilicity of the material [48, 49]. At 298 K, the CHS and PLA exhibited a dispersive surface energy of 41.02 mJ/m$^2$ and 37.62 mJ/m$^2$, respectively. PLA–CHS composites modified with 0.4 and 0.8% of chitosan present a lower dispersive energy, when compared to the raw materials may be due to the crosslinking of polymer chains [50]. It was observed that the hydrophobicity of the composites enhanced slightly with the increase in filler concentration. Higher filler concentration (0.8 wt% chitosan) presented a smaller entropic factor (0.11 mJ m$^{-2}$/K) than that of 0.4% filler added composites, which indicates the increase of crosslinking efficiency in PLA-0.8 wt% chitosan (free chains–higher entropy). The surface area of the samples range between 0.83 and 3.07 m$^2$/g and the monolayer capacity range between 2.18 and 8.08 µmol/g. The addition of chitosan decreases the PLA surface area (particles increasing) and decrease the DP (porosity decreasing) due probably to the reticulation increasing with a more compact particles formation. Monolayer capacity ($n_m$) is the maximum number of adsorption sites for a monolayer coverage. The diffusion coefficient ($D_p$) is a physical constant dependent on molecule size and other properties of the diffusing substance as well as on temperature and pressure. It is also measure of the porosity of the composite scaffold. The decrease in diffusion coefficient also supports the decrease in porosity of the scaffolds with the increase in addition of chitosan. The interactions between the chitosan and the polar probes were found to be very weak and the values of $K_A$ and $K_B$ is very small. All PLA sample exhibited a basic character. PLA with 0.4 % chitosan show a stronger basic character ($K_B/K_A = 1.75$) probably due to the lower crosslinking which expose more the C = O, C–O–C and $NH_2$ groups.

### 4.5 Zeta potential measurements

Surface charges of the PLA, CHS and PLA–CHS composites were determined by zeta (ζ) potential measurements. The magnitude of the zeta potential indicates the degree of electrostatic repulsion between adjacent, similarly charged particles in dispersion or suspension. Higher zeta potential value (despite of the magnitude) refers to the stability of the suspension [51]. As seen in Table 4, it was clear that chitosan possess a high stability ($\zeta = 60.2$), since zeta potential is directly proportional to the stability of nano particles. This may be because of the ionization of free amino groups of chitosan in aqueous medium to ammonium ion ($-NH_2$ to $-NH_3^+$). But the stability of PLA chitosan composite is very low compared to chitosan. This is due to the decrease in the number of ionizable primary amino groups. But with increase in the of chitosan content the zeta potential value first increases and at higher loading low zeta potential value observed due to poor interaction. That is 0.4 wt% of CHS loaded PLA possess better interaction than other loadings.

### 4.6 Contact angle measurements

Hydrophobicity of the composites were evaluated by the contact angle measurements. Figure 7 shows the results obtained for the composites with filler concentration. It was found that the values (contact angles) increased with the increase in filler content, which indicates the increase of hydrophobicity of the material (see Fig. 7). This may be due to the decrease in the surface roughness which can lead to an increase of contact angles, thereby decreasing the wetting ability of the fibrous membrane. The results was close agreement with the IGC results, showing the decrease of surface free energy of the composites with increase in filler content. The variation of surface free energy with respect to filler loading is shown in Fig. 8. Here the hydrophobicity results from a combination of decreased fiber diameter and low surface energy [52].

### 4.7 Cytotoxicity studies

The results of viability/cytotoxicity assays demonstrate that there was a significant statistical difference ($p \leq 0{,}000$) between the cell viability in PLA and all PLA/CHS membranes, regardless of their concentration. There was no statistical difference between the levels of cell viability exhibited by PLA/CHS membranes at concentrations of 0.2, 0.4 and 0.6%. Although lower than the control and PLA groups, they are compatible with levels still considered non-cytotoxic. The PLA/CHS 0.8% membranes presented levels of viability significantly lower than the other PLA/CHS groups and close to the value from which a cytotoxic effect will be considered (≤70% of cell viability). The results

surely indicate that PLA/CHS membranes, at concentrations of 0.2, 0.4, and 0.6%, are non-cytotoxic. This characteristic enables to explore its potential as a biomaterial for biomedical applications. PLA and CHS are known non-cytotoxic components. Taking this into account, it is recommended to consider the possibility that residues of solvent still exist in CHS (acetic acid) and may be responsible for the cytotoxic effect detected in the samples, especially in the higher concentrations of CHS.

## 5 Conclusion

Here, we have successfully fabricated electrospun PLA –CHS mats. At 0.4 wt% concentration of chitosan we got a uniform diameter for the fibres. FTIR and TGA results revealed that there is only weak interaction between the filler and the matrix. IGC as well as contact angle measurements showed that the membranes were hydrophobic and hydrophobicity of the membrane increases with increase in filler content. The decrease in surface roughness was attributed to the decreased fiber diameter and low surface energy and hence hydrophobicity. The cell viability studies revealed that PLA and PLA–CHS upto 0.6% were noncytotoxic and can be used as a potential biomaterial for biomedical applications.

**Acknowledgements** The first author is grateful to the Council for Scientific and Industrial Research (CSIR) Government of India and University Grants Commission for the financial funding for this research by giving Junior Research Fellowship. We thank Dr. Jayakumar Rangasamy for his valuable advices regarding zeta potential measurement.

### Compliance with ethical standards

**Conflict of interest** The authors declare that they have no conflict of interest.

## References

1. Vroman I, Tighzert L. Biodegradable polymers. Materials. 2009;2:307–44.
2. Adeosun SO, Lawal GI, Balogun SA, Akpan EI. Review of green polymer nanocomposites. J Miner Mater Charact Eng. 2012;11:385.
3. Stevens ES. Green plastics: an introduction to the new science of biodegradable plastics. Binghamton: Princeton University Press; 2002.
4. Kulkarni Vishakha S, Butte Kishor D, Rathod Sudha S. Natural polymers–A comprehensive review. Int J Res Pharm Biomed Sci. 2012;3:1579–613.
5. Grujic R, Vukic M, Gojkovic V. Application of biopolymers in the food industry. In: Pellicer E, Nikolic D, Sort J, Baró M, Zivic F, Grujovic N, et al, editors. Advances in applications of industrial biomaterials. Cham: Springer; 2017. p. 103–19.
6. Azeredo HM, Rosa MF, Mattoso LH. Nanocellulose in bio-based food packaging applications. Ind Crops Prod. 2017;97:664–71.
7. Torino MI, Font de Valdez G, Mozzi F. Biopolymers from lactic acid bacteria. Novel applications in foods and beverages. Front Microbiol. 2015;6:834.
8. Kas HS. Chitosan: properties, preparations and application to microparticulate systems. J Microencapsul. 1997;14:689–711.
9. Sangeetha Y, Meenakshi S, SairamSundaram C. Corrosion mitigation of N-(2-hydroxy-3-trimethyl ammonium) propyl chitosan chloride as inhibitor on mild steel. Int J Biol Macromol. 2015;72:1244–9.
10. Riedel U, Nickel J. Natural fibre-reinforced biopolymers as construction materials–new discoveries. Die Angew Makromol Chem. 1999;272:34–40.
11. Thoen J, Busch R. Industrial chemicals from biomass–Industrial concepts. In: Birgit Kamm, Patrick R Gruber, Michael Kamm, editors. Biorefineries-industrial processes and products: status quo and future directions. Wiley-VCH Verlag GmbH, Weinheim; 2006, p. 347–65.
12. Aeschelmann F, Carus M. Biobased building blocks and polymers in the world: capacities, production, and applications–status quo and trends towards 2020. Ind Biotechnol. 2015;11:154–9.
13. Jiang T, Abdel-Fattah WI, Laurencin CT. In vitro evaluation of chitosan/poly (lactic acid-glycolic acid) sintered microsphere scaffolds for bone tissue engineering. Biomaterials. 2006;27:4894–903.
14. Henton DE, Gruber P, Lunt J, Randall J. Polylactic acid technology. Nat Fibers Biopolym biocomposites. 2005;16:527–77.
15. Fortunati E, Luzi F, Puglia D, Petrucci R, Kenny JM, Torre L. Processing of PLA nanocomposites with cellulose nanocrystals extracted from Posidonia oceanica waste: Innovative reuse of coastal plant. Ind Crops Prod. 2015;67:439–47.
16. McCarthy CW, Ahrens DC, Joda D, Curtis TE, Bowen PK, Guillory RJ, et al. Fabrication and short-term in vivo performance of a natural elastic lamina–polymeric hybrid vascular graft. ACS Appl Mater Interfaces. 2015;7:16202–12.
17. Lasprilla AJ, Martinez GA, Lunelli BH, Jardini AL, Maciel Filho R. Poly-lactic acid synthesis for application in biomedical devices—a review. Biotechnol Adv. 2012;30:321–8.
18. Sakai R, John B, Okamoto M, Seppälä JV, Vaithilingam J, Hussein H, et al. Fabrication of polylactide-based biodegradable thermoset scaffolds for tissue engineering applications. Macromol Mater Eng. 2013;298:45–52.
19. Li G, Wang ZX, Fu WJ, Hong BF, Wang XX, Cao L, et al. Introduction to biodegradable polylactic acid ureteral stent application for treatment of ureteral war injury. BJU Int. 2011;108:901–6.
20. Yong SK, Shrivastava M, Srivastava P, Kunhikrishnan A, Bolan N. Environmental applications of chitosan and its derivatives. Rev Environ Contam Toxicol. 2015;233:1–43.
21. Kumar PS, Srinivasan S, Lakshmanan VK, Tamura H, Nair SV, Jayakumar R. β-Chitin hydrogel/nano hydroxyapatite composite scaffolds for tissue engineering applications. Carbohydr Polym. 2011;85:584–91.
22. Kavitha K, Keerthi TS, Mani TT. Chitosan polymer used as carrier in various pharmaceutical formulations: brief review. Int J Appl Biol Pharm Techol. 2011;2:249–58.
23. Wan AC, Tai BC. CHITIN—a promising biomaterial for tissue engineering and stem cell technologies. Biotechnol Adv. 2013;31:1776–85.
24. Yang TL. Chitin-based materials in tissue engineering: applications in soft tissue and epithelial organ. Int J Mol Sci. 2011;12:1936–63.
25. Bartley J. Should chitosan and tranexamic acid be combined for improved hemostasis after sinus surgery? Med Hypotheses. 2013;81:1036–8.

26. Bojar W, Kucharska M, Ciach T, Koperski Ł, Jastrzębski Z, Szałwiński M. Bone regeneration potential of the new chitosan-based alloplastic biomaterial. J Biomater Appl. 2014;28:1060–8.
27. Bhardwaj N, Kundu SC. Electrospinning: a fascinating fiber fabrication technique. Biotechnol Adv. 2010;28:325–47.
28. Tomaszewski W, Szadkowski M. Investigation of electrospinning with the use of a multi-jet electrospinning head. Fibres Text East Eur. 2005;13:22.
29. Ohkawa K, Cha D, Kim H, Nishida A, Yamamoto H. Electrospinning of chitosan. Macromol Rapid Commun. 2004;25:1600–5.
30. Kriegel C, Kit KM, McClements DJ, Weiss J. Influence of surfactant type and concentration on electrospinning of chitosan–poly (ethylene oxide) blend nanofibers. Food Biophys. 2009;4:213–28.
31. Au HT, Pham LN, Vu TH, Park JS. Fabrication of an antibacterial non-woven mat of a poly (lactic acid)/chitosan blend by electrospinning. Macromol Res. 2012;20:51–58.
32. Van der Schueren L, De Meyer T, Steyaert I. et al. Polycaprolactone and polycaprolactone/chitosan nanofibres functionalised with the pH-sensitive dye Nitrazine Yellow. Carbohydr Polym. 2013;91:284–93.
33. Sundaramurthi D, Vasanthan KS, Kuppan P, Krishnan UM, Sethuraman S. Electrospun nanostructured chitosan–poly (vinyl alcohol) scaffolds: a biomimetic extracellular matrix as dermal substitute. Biomed Mater. 2012;7:045005.
34. Sonseca A, Peponi L, Sahuquillo O, Kenny JM, Giménez E. Electrospinning of biodegradable polylactide/hydroxyapatite nanofibers: study on the morphology, crystallinity structure and thermal stability. Polym Degrad Stab. 2012;97:2052–9.
35. Xu C, Yang F, Wang S, Ramakrishna S. In vitro study of human vascular endothelial cell function on materials with various surface roughness. J Biomed Mater Res A. 2004;71:154–61.
36. Megelski S, Stephens JS, Chase DB, Rabolt JF. Micro-and nanostructured surface morphology on electrospun polymer fibers. Macromolecules. 2002;35:8456–66.
37. Kim GM, Michler GH, Pötschke P. Deformation processes of ultrahigh porous multiwalled carbon nanotubes/polycarbonate composite fibers prepared by electrospinning. Polym (Guildf). 2005;46:7346–51.
38. Zheng J, Zhang H, Zhao Z, Han CC. Construction of hierarchical structures by electrospinning or electrospraying. Polym (Guildf). 2012;53:546–54.
39. Augustine R, Kalarikkal N, Thomas S. An in vitro method for the determination of microbial barrier property (MBP) of porous polymeric membranes for skin substitute and wound dressing applications. Tissue Eng Regen Med. 2015;12:12–19.
40. Yang T, Wu D, Lu L, Zhou W, Zhang M. Electrospinning of polylactide and its composites with carbon nanotubes. Polym Compos. 2011;32:1280–8.
41. Zhao R, Li X, Sun B, Zhang Y, Zhang D, Tang Z, et al. Electrospun chitosan/sericin composite nanofibers with antibacterial property as potential wound dressings. Int J Biol Macromol. 2014;68:92–97.
42. Furukawa T, Sato H, Murakami R, Zhang J, Duan YX, Noda I, et al. Structure, dispersibility, and crystallinity of poly (hydroxybutyrate)/poly (L-lactic acid) blends studied by FT-IR microspectroscopy and differential scanning calorimetry. Macromolecules. 2005;38:6445–54.
43. Chu Z, Zhao T, Li L, Fan J, Qin Y. Characterization of antimicrobial poly (lactic acid)/nano-composite films with silver and zinc oxide nanoparticles. Materials. 2017;10:659.
44. Morán JI, Alvarez VA, Cyras VP, Vázquez A. Extraction of cellulose and preparation of nanocellulose from sisal fibers. Cellulose. 2008;15:149–59.
45. Mofokeng JP, Luyt AS, Tábi T, Kovács J. Comparison of injection moulded, natural fibre-reinforced composites with PP and PLA as matrices. J Thermoplast Compos Mater. 2012;25:927–48.
46. Haafiz MM, Hassan A, Zakaria Z, Inuwa IM, Islam MS, Jawaid M. Properties of polylactic acid composites reinforced with oil palm biomass microcrystalline cellulose. Carbohydr Polym. 2013;98:139–45.
47. Xu J, Zhang J, Gao W, Liang H, Wang H, Li J. Preparation of chitosan/PLA blend micro/nanofibers by electrospinning. Mater Lett. 2009;63:658–60.
48. Cordeiro N, Gouveia C, Moraes AG, Amico SC. Natural fibers characterization by inverse gas chromatography. Carbohydr Polym. 2011;84:110–7.
49. Deepa B, Abraham E, Cordeiro N, Mozetic M, Mathew AP, Oksman K, et al. Utilization of various lignocellulosic biomass for the production of nanocellulose: a comparative study. Cellulose. 2015;22:1075–90.
50. Deepa B, Abraham E, Pothan LA, Cordeiro N, Faria M, Thomas S. Biodegradable nanocomposite films based on sodium alginate and cellulose nanofibrils. Materials. 2016;9:50.
51. Hanaor D, Michelazzi M, Leonelli C, Sorrell CC. The effects of carboxylic acids on the aqueous dispersion and electrophoretic deposition of $ZrO_2$. J Eur Ceram Soc. 2012;32:235–44.
52. Han D, Steckl AJ. Superhydrophobic and oleophobic fibers by coaxial electrospinning. Langmuir. 2009;25:9454–62.